Anode/cathode Dual-purpose Aluminum Current Collectors for Aqueous Zinc-ion Batteries

Ruijie Zhu †, Zetao Xiong †, Huijun Yang, Ning Wang, Sho Kitano, Chunyu Zhu*, Yoshitaka Aoki, and Hiroki Habazaki.*

Ruijie Zhu - Graduate School of Chemical Sciences and Engineering, Hokkaido University, Sapporo, Hokkaido 060-8628, Japan

Zetao Xiong - Graduate School of Chemical Sciences and Engineering, Hokkaido University, Sapporo, Hokkaido 060-8628, Japan

Huijun Yang - National Institute of Advanced Industrial Science and Technology (AIST), 1-1-1, Umezono, Tsukuba 305-8568 Japan.

Ning Wang - Huangpu Hydrogen Energy Innovation Centre, School of Chemistry and Chemical Engineering, Guangzhou University, Guangzhou 510006, China

Sho Kitano - Division of Applied Chemistry, Faculty of Engineering, Hokkaido University, Sapporo, Hokkaido 060-8628, Japan

Chunyu Zhu - School of Low-carbon Energy and Power Engineering, China University of Mining and Technology, Xuzhou 221116, China

Yoshitaka Aoki - Division of Applied Chemistry, Faculty of Engineering, Hokkaido University, Sapporo, Hokkaido 060-8628, Japan

Hiroki Habazaki - Division of Applied Chemistry, Faculty of Engineering, Hokkaido University, Sapporo, Hokkaido 060-8628, Japan

Corresponding Author

* Chunyu Zhu - School of Low-carbon Energy and Power Engineering, China University of Mining and Technology, Xuzhou 221116, China

* Huijun Yang - National Institute of Advanced Industrial Science and Technology (AIST), 1-1-1, Umezono, Tsukuba 305-8568 Japan.

E-mail: zcyls@cumt.edu.cn

yang.hj@aist.go.jp

Keywords

aqueous zinc-ion battereies, magnetron sputtering, niobium, corrosion resistance, current collector.

,

Abstract

Rechargeable aqueous zinc-ion batteries (RAZIBs), which use non-flammable aqueous electrolytes and low-cost electrode materials, show great potential to boost the development of safe, cost-effective, and highly efficient energy storage for whatever the mass adoption of electric vehicles or the large-scale energy storage of solar photovoltaic systems. The adoption of lightweight and inexpensive aluminum (Al) as current collectors seems to be a good vision, but Al exhibits an easily-corroded nature and a high impedance in aqueous electrolytes, making it a challenge to realize the utilization of Al current collector in RAZIBs. In this study, through the direct current magnetron sputtering, niobium (Nb) coated Al (Al-Nb) foils were prepared, which showed superior corrosion-resistance in aqueous solution, while maintaining a satisfying electronic conductivity. Moreover, the Al-Nb foils could be adopted to both anode and cathode current collectors while exhibiting high coulombic efficiency and good cycling stability even when they were tested under a condition that can meet the real-world application demands, e.g., the Zn||Al-Nb half cell showed an average coulombic efficiency of 99.17% in 320 cycles under a current density of 25 mA cm^{-2} and a galvanizing capacity of 6.25 mAh cm^{-2}. The superior performance of the modified Al current collectors may mark a significant step towards the development of high-energy-density aqueous

batteries.

Introduction

Aqueous zinc-based batteries (AZBs), known as reliable portable power, have served mankind for hundreds of years.[1, 2] Adequate reasons for utilizing zinc (Zn) metal in battery chemistry not only come from its low-cost and abundance, e.g., Li~USD$19.2 kg^{-1} vs. Zn~USD$2.4 kg^{-1}, but also for its high capacity and low potential, i.e., 5854 mA h cm^{-3} and -0.76 V vs standard hydrogen electrode (SHE).[3-5] Up to now, the family of AZIBs includes Zn-vanadium pentoxide (V_2O_5) batteries, Zn-manganese dioxide (MnO_2) batteries, Zn- nickel oxide hydroxide (NiOOH) batteries, Zn- iodine (I_2) batteries, Zn-oxygen (O_2) batteries, etc.[6-13] Most of them have satisfactory energy densities and are much safer than current lithium-ion batteries (LIBs) or lead-acid batteries because the AZBs are virtually non-flammable with aqueous electrolytes. However, the AZBs currently occupying the market are still primary batteries based on alkaline electrolytes. In many cases, using rechargeable aqueous zinc-ion batteries (RAZIBs) to replace primary batteries will effectively reduce environmental damage. Unfortunately, RAZIBs are still facing many challenges, including the growth of Zn dendrites during repeated electroplating and striping, side reactions between Zn metal

and electrolyte, gas evolution reactions, and unsatisfying capacity retention. [14-19] Many efforts have been made toward developing cathode materials with superior performance or finding solutions to achieve stable Zn anodes.[20-23] However, one inconspicuous but very important issue that has not been paid much attention to is the current collectors used in RAZIBs. Due to the corrosiveness of protic solvents to metals and the sensitivity of water splitting reaction, only highly conductive materials, which have excellent corrosion resistance and a lack of catalytic activity for water electrolysis, are suitable as current collectors in aqueous batteries. Therefore, only a few materials, including stainless steel,[24] copper (only for the anode),[25] nickel,[26] titanium [27], and carbon sheets[28], have been successfully employed as current collectors in AZBs so far.[29] Aluminum (Al) current collectors are widely used in LIBs, and the light-weight, low-cost, and highly-conductive nature makes Al the best candidate for current collectors. Unfortunately, because Al is inevitably corroded in aqueous solutions, it is difficult to directly use Al as the current collector for AZBs. Niobium (Nb) is known for its excellent corrosion resistance because of the formation of a thin and stable protective passive film in aqueous solutions with a wide pH range.[30, 31] Recently, some studies also pointed out that Nb_2O_5 is a good material for inducing uniform Zn deposition. [32] Moreover, Nb is able to form a dense and well-adhered coating on the surface of Al_2O_3

without damaging the substrate or the coating itself, even when the Al_2O_3 has a unique 3D structure, which allows Nb to form a superior anti-corrosion coating on the Al foil surface that is difficult to achieve with other coating methods.[33]

Here, through a physical vapor deposition (PVD) method, thin Nb layers are magnetron sputtered to Al foils to make the Nb coated Al foils (Al-Nb foils), which are successfully used as the dual-purpose current collectors for both anode and cathode in RAZIBs **(Figure S1)**. The magnetron sputtered Nb coating layer eliminates the influence of the insulating oxide layer on Al surface; the extremely thin oxide layer on the surface of the Nb layer can resist the corrosion of the current collector during the charging and discharging process while ensuring an excellent electronic conductivity of the current collector. PVD is a well-established technology suitable for industrial production. Since the RAZIBs supported by Al-Nb show excellent electrochemical cyclic performance and improved energy density in this study, the use of Nb coating may provide a new opportunity for realizing real-world applicable RAZIBs by providing light-weight current collectors.

2. Results and discussion

As shown in **Figure 1a**, the Al-Nb foil was prepared by depositing Nb metal onto the

surface of Al foil. Considering that adjusting the time of magnetron sputtering would result in different thicknesses of Nb coating, we chose the sample with a moderate thickness to characterize the structure information of the Al-Nb foil. The as-prepared Al-Nb foil has a flat and clean surface, as shown in **Figure S2.** The Al-Nb foil sample, which was obtained by sputtering Nb metal to Al foil for 15 min at the voltage of 250 V, was firstly treated by a rotary microtome to possess a sample for scanning transmission electron microscopy (STEM) observation. As shown in **Figure 1b**, a dense layer consisting of Nb and O is tightly adhered to the surface of the Al substrate. The thickness of Nb coating is around 310 nm, while the composition analysis shows that the atom ratios of Nb and O in the Nb coating layer are 86.8% and 12%, respectively **(Figure S3)**. The electrron diffraction pattern of the Nb coating revealed a bcc pattern; thus, the coating was metallic Nb supersaturated with oxygen. The oxygen may be originated mainly from the moisture impurity in the sputtering chamber. High-resolution transmission electron microscopy (HRTEM) observation was employed to detect the surface and interface information of the Al-Nb foil. As shown in **Figure 1c**, the top surface of the Nb coating is covered by a thin but dense oxide layer, which is naturally formed in the air with a thickness of several nanometers. Amorphous interphase with a thickness of about 5 nm was observed between the Al substrate and the Nb coating in

Figure 1d. The amorphous interphase, possibly sourced from the naturally formed oxide layer on Al foil, tightly bonds the Al substrate and the Nb coating.[34, 35] The structure model of the Al-Nb foil is depicted in **Figure 1e.** To further understand the structure, we used Auger electron spectroscopy (AES) and electron energy loss spectroscopy (EELS). The AES depth profile of the Nb coating is shown in **Figure 1f**; a 30 s argon-ion (Ar^+) etching was processed before every cycle except the first one. The etching rate is 0.44 nm min^{-1} (calculated by etching SiO_2). Two peaks belonging to Nb (MNN electronic transition,195.5 eV) and O (KLL electronic transition, 506.8 eV), respectively, are marked in the figure. The intensity of the Nb MNN peak shows a trend of increasing with the etching, whereas the intensity of the O KLL peak shows an exact opposite trend, indicating that the passivation layer is a thin oxides film with a thickness of several nanometers. Line profile EELS spectra, recorded from the top of the orange line to the bottom of the orange line in **Figure 1(b_1)**, are presented in **Figure 1g** and **Figure 1h**. Total 100 points were recorded during the scanning. The first and the second points recorded at position A as marked in **Figure 1(b_1)** are shown in **Figure 1g**. As depicted in **Figure 1g**, the peak at roughly 245 eV is regarded as the recorded Nb-$M_{4,5}$ edge, caused by the transition of 3d electrons to the unoccupied 4f and 5p states. The peak shows a typical shape of Nb^{5+}, indicating that the main composition of the thin

oxides layer is Nb_2O_5.[36] Moreover, only the first and the second points recorded a similar curve during the EELS measurement, demonstrating that the thickness of the oxide layer is about several nanometers **(Figure S4)**. Three points recorded at position B, as marked in Figure 1(b1), are shown in Figure 1h, which reveals the interphase composition. At the first point, the two peaks for the Al-$L_{2,3}$ edge can be clearly observed, indicating that the simultaneous presence of Al_2O_3 and metallic Al in the interphase layer. The second and third points only show a less-obvious Al peak, demonstrating that the interphase thickness agrees with the results obtained from HRTEM observation. The composite form of both metal and oxide at the interface ensures a reliable electronic path between the Nb coating and the Al substrate. Furthermore, the extremely thin upper surface oxide layer will not unduly damage the electronic conductivity of the Al-Nb foil, which gives Al-Nb the basic possibility of being employed as a current collector.

As for the electrochemical measurement, we first studied the electrochemical characteristics of Al-Nb foil when it was used as the anode current collector. Electrochemical impedance spectroscopy (EIS) was employed to understand the difference between three kinds of metallic substrates. Here, two-electrode cells were assembled using Zn foil as a counter electrode and Cu foil or Al-Nb foil or Al foil as a

working electrode. 2 M $ZnSO_4$ aqueous solution (aq.) was used as the electrolyte. As shown in **Figure 2a**, the Al foil exhibits large interfacial impedance, the Al-Nb foil shows a moderate value, and the Cu foil shows the lowest resistance. The highest resistance implies that the surface of Al foil is passivated by forming a thicker passive film in the aqueous solution, and this insulating passivation layer may be the culprit of the markedly reduced conductance. The conductive atomic force microscopy (c-AFM) observation also demonstrates the surface conductivity of different metal surfaces. As shown in **Figure S5**, the surfaces of both Al-Nb foil and Cu foil show a high number of high conductivity sites that are suitable for electrochemical reactions, while the conductivity on Al surface looks bad. We further conducted linear sweep voltammetry (LSV) tests for Zn plating on different substrates to discuss the difficulty of Zn deposition on different metals. As shown in **Figure S6**, in order to avoid the possible influence from the HER, the onsetpotential of the galvanizing is specified as the voltage at which the current density is -0.25 mA cm^{-2}. The onset potential of the growth of Zn on Cu foil, Al-Nb foil, and Al foil are -1.01 V, -1.02 V, and -1.07 V (vs. Ag/AgCl), respectively. The results indicate that the Cu foil seeds the deposition of Zn well, and the nucleation of Zn on the Al-Nb is slightly influenced due to the relatively high impedance. The significant lagging of the deposition onset potential and the low

galvanizing current demonstrates that both the nucleation and the growth of Zn are greatly hindered by the passive film on the Al foil. Hence, we arrange the growing difficulty of Zn on three different substrates as Al > Al-Nb ≈ Cu, among which the slightly higher overpotential of Al-Nb than Cu confirms our point of view that the passive film on Al-Nb will not seriously hinder the galvanizing on Al-Nb foil. The other LSV test for Zn plating/stripping procedure on different metals was also employed to discussing whether the Nb coating can optimize the galvanizing reversibility on Al foil. As shown in **Figure 2b**, the sweep started from -0.5 V (vs. Zn/Zn^{2+}) and ended at 0.5 V. The anodic peak that appears in the positive potential region represents the stripping capability of Zn on different substrates. The ratio of the capacity generated by the negative current to the positive current reflects the reversibility of the Zn deposition. The ratio of negative/positive capacity for the Cu foil, the Al-Nb foil, and the Al foil are calculated to 99.4%, 98.1%, and 8%, respectively. An apparent conclusion is drawn after comparing the capacity ratio; that is, the Zn deposited on the Al foil is difficult to be dissolved due to the blocked electron pathway, while the stripping of Zn from Al-Nb foil shows a Zn plating/stripping reversibility that is close to Cu foil. The above discussion shows that introducing Nb coating will eliminate the conductivity degradation caused by the surface passivation of Al. Another serious problem is the

formation and accumulation of zinc hydroxide sulfate ($Zn_4(OH)_6SO_4$ xH_2O, (ZHS)) in the electrolytes, which will damage the performance of the Zn anode.[37] Here, by carrying out an LSV test in a K_2SO_4 aqueous solution, we first examine the hydrogen evolution reaction (HER) activity of different substrates. H_2SO_4 was added to the K_2SO_4 aqueous solution to obtain a faintly acidic solution whose pH is consistent with that of the $ZnSO_4$ aqueous solution（pH≈4.1）. As shown in **Figure 2c**, the potentials required for the Cu foil, the Al-Nb, and the Al foil to achieve a current density of 1 mA cm^{-2} are -1.03 V, -1.54 V, and -1.59 V (vs. Ag/AgCl), respectively. In the range of Zn deposition potentials (i.e. -0.97 V to -1.1 V vs. Ag/AgCl), the HER can hardly takes place on the surface of Al-Nb foil because no significant current can be observed in this range. This indicates that the Al-Nb foil is far superior to Cu foil in inhibiting the hydrogen evolution in such an acidic condition. Then, we employed a simple potentiostatic test to examine the formation of ZHS on different substrates in a 2 M $ZnSO_4$ aqueous electrolyte when the electrodeposition of Zn is absent. Zn||substrate two-electrode cells, which employed the Zn foil as counter electrode and the metal substrate as working electrode, were used in the test. The potential was controlled to 0 V (vs. Zn/Zn^{2+}) during the test. As shown in **Figure 2d**, tens of micro-ampere current were monitored on the Cu foil during the 50 hours test, whereas only 2 uA were observed on the Al-Nb foil. On

the Al-Nb foil, the current recorded is considered mainly caused by the slight HER, but for the Cu foil, the underpotential deposition of Zn can be also regarded as a source of the current.[38] Hence, the HER on the Cu can be also partially influenced by the deposited Zn atom layer. The progress of the HER will increase the OH^- concentration at the electrode-electrolyte interface and promote the formation of ZHS: [39, 40]

$2H_2O + 2e^- \rightarrow H_2 + 2OH^-$ (Equation 1)

$4Zn^{2+} + 6OH^- + {SO_4}^{2-} + xH_2O \rightarrow Zn_4(OH)_6SO_4 \cdot xH_2O$ (Equation 2)

The increase in OH- concentration leads to severe corrosion to the Cu foil, and causes a large amount of ZHS to accumulate on its surface, which results in the significant corrosion current. We examined the surface condition of the metal substrates by scanning electron microscopy (SEM) and energy-dispersive X-ray spectroscopy (EDS), and the results are presented in **Figure 2e** and **Figure S7.** Numerous flaky ZHS covers the upper surface of the Cu foil, and the surface of Al foil is also full of ZHS residues. This shows that when used as anode current collectors, a large amount of ZHS will generate on both Al foil and Cu foil, and the accumulation of ZHS will inevitably damage the electrochemical performance of the Zn metal anode.[41] By contrast, ZHS is barely observed on the surface of Al-Nb foil, which is consistent with the extremely low current in the potentiostatic tests. The difference between the Al foil and the Al-Nb

foil can be explained by the difference in the point of zero charge (PZC) of Al_2O_3 and Nb_2O_5. In aqueous solution, the PZC of Al_2O_3 generally appears in an alkaline environment, for example, the PZC of α-Al_2O_3 is commonly recorded when pH = 9.1.[42, 43] This PZC value causes the surface of Al foil is charged thus the ion in the electrolyte can be easily attracted and precipitated onto the surface to form the ZHS. In reverse, the PZC of Nb_2O_5 was considered to appear when pH = 4.1, which is quite close to the pH recorded in the $ZnSO_4$ electrolyte. **[44]** The surface charge density of the Al-Nb is close to 0, which makes the sedimentation of ZHS difficult, allowing Al-Nb to maintain a clean surface. These results show that when being used as anode current collectors, a large amount of ZHS will generate on both Al foil and Cu foil, and the accumulation of ZHS will damage the electrochemical performance of the Zn metal anode. By contrast, ZHS is barely observed on the surface of Al-Nb foil, which is also consistent with the extremely low current in the potentiostatic tests.

Repeated Zn plating/stripping tests on the substrates will intuitively reflect the cycling performance of the anode side when different substrates are used as anode current collectors. As shown in **Figure 3a**, Al||Zn, Al-Nb||Zn, Cu||Zn half-cells were assembled and tested under a current density of 25 mA cm^{-2}; here, the areal capacity of Zn deposition was controlled to 6.25 mA h cm^{-2} in each cycle. The Al||Zn cell only has an

initial coulombic efficiency (I.C.E.) of 28.99 %, and 49.68 %, 75.41 % for the next two cycles. The badly low I.C.E. indicates that the high-resistance passivation layer on the Al metal significantly affects the electrochemical dissolution of the as-deposited Zn metal. The Cu||Zn cell and the Al-Nb||Zn cell show high I.C.E. of 96.60 % and 93.91 %, respectively. The higher I.C.E. on Cu foil is due to the unobstructed electronic pathways between Cu and Zn during the initial cycle.

Regarding the whole test, the Al-Nb||Zn cell provides a stable average coulombic efficiency (A.C.E.) of 99.17 %, while the Cu||Zn cell offers an A.C.E. of 99.34%. The high A.C.E. values show that Al-Nb owns the ability to guarantee the deposition reversibility of Zn comparable to that of Cu foil. It is also worth noting that the Al-Nb||Zn cell has a life span of 320 cycles, while the Al||Zn cell and the Cu||Zn cell survive for 49 cycles and 161 cycles before short-circuiting, respectively. Voltage profiles of the three cells are shown in **Figure 3b** and **3c**. As presented in Figure 2b, extremely high overpotential can be observed when Zn coating is stripped from Al foil, indicating that the electrochemical dissolution of Zn is severely hindered by the insulating passivation layer. Comparing the performance of Al-Nb foil and Cu foil, it can be found that the overpotential of Zn deposition on Al-Nb is slightly higher than that of Cu, which can be ascribed to the relatively higher electrochemical impedance of

Al-Nb. Due to the similar reason, the Zn stripping overpotential of Al-Nb is also slightly higher than that of Cu, but as we pointed out in Figure 2b and 2c that the stripping overpotential (134 mV and 132 mV) at the capacity of 3.125 mAh cm^{-2} does not change during the 300 cycles, demonstrating that the Al-Nb foil can maintain a good surface condition to support the electrochemical cycling of Zn metal anode. Then, we took the optical photos and SEM images for different substrates after one cycle of Zn plating-stripping to confirm the surface condition change during the half-cell tests. As shown in **Figure 3d** and **Figure S8**, the Cu surface is covered by messy ZHS, which is the primary reason for the damaged cycling performance. As a comparison, a clean surface with a metallic luster, which belongs to the Al-Nb foil after a one-time galvanizing-stripping cycle, is shown in **Figure 3e**. In addition, optical photos of three different substrates after Zn deposition or Zn stripping are shown in **Figure S9**. It can be seen that Al-Nb exhibits the best corrosion resistance and the resistance to ZHS generation among the three substrates. It is also worth mentioning that the plating of Zn on the Al-Nb foil is also flat and smooth **(Figure S10)**, but the good deposition performance is not only due to its anti-corrosion properties but also due to the high current densities, by which the growth of dendritic crystals can be greatly suppressed.[45, 46]

X-ray photoelectron spectroscopy (XPS) depth profile was employed to detect the

surface composition of the substrates after Zn stripping. As shown in **Figure 3f** and **3g**, the ZHS residues on Cu foil are present even at a depth of 140 nm, while the thickness of ZHS on Al foil is around 50 nm. No information from Cu 2p orbital was monitored within 80 nm depth of the Cu surface (**Figure S11**), indicating that the ZHS layer formed on the Cu surface is very dense; thus, the current distribution and the migration of Zn atoms on the Cu surface would be undoubtedly influenced. The Al-Nb foil keeps clean after electrochemically stripping the as-deposited Zn coating, and the continuously visible peak from the Nb 2p orbital also confirms this conclusion (**Figure S11)**, by which the galvanizing and stripping can be carried out in a highly uniform way, as we depicted in **Figure 3i.** Reversibility tests for Zn deposition under different current densities are shown in **Figure S12** and **Figure S13**. It can be found that the coulombic efficiency of Al-Nb foil is slightly lower than that of Cu foil at low current densities, but a high value can be still maintained. Under the high current density and large deposition capacity, the Al-Nb can effectively reduce the proportion of side reactions presented on the collector surface, which makes Al-Nb exhibit excellent reversibility and lifetime under high current. Moreover, electrodepositing Zn under a current density of 0.1 mA cm^{-2} will not break the Nb coating layer, indicating that the Nb coating can withstand the possible alloying reaction, thus guaranteeing the performance of Zn anode in long-

term cycling (**Figure S14)**. To further demonstrate the excellent performance of Nb coating in reducing ZHS formation, ex-situ XRD was applied to observe the accumulation of ZHS on different substrates during repeated Zn plating/stripping. As shown in **Figure 4a, Figure S15** and **Figure S16,** peaks that belong to ZHS appeared on the Al-Nb after the first and the second Zn deposition, but after Zn stripping, there was almost no residual by-product on the surface of Al-Nb foil. After a certain number of Zn plating/stripping cycles, the Al-Nb foil remained its highly clean surface. This is attributed to the relatively low HER activity of Nb_2O_5 and the PZC close to the pH, which together make it difficult for ZHS to accumulate on the Al-Nb surface. In contrast, ZHS is always appear on the surface of Cu (**Figure 4b**). And as the cycle proceeds, ZHS will continue to accumulate on the Cu surface, resulting in great risk of Zn dendrite formation on Cu, which is the reason why Cu foil shows a much lower lifetime than Al-Nb in the half-cell test. DFT simulation was also employed to confirm the conclusion. As shown in **Figure 4c** and **Figure 4d**, for the three different substrates discussed, Cu exhibited the best catalytic performance for HER because it shows the lowest free energy barrier (0.14 eV) for the HER. The HER activity of Nb metal is also lower than Cu, while the HER activity of Nb_2O_5 and Al_2O_3 was much lower than that of the two metals. This suggests that Nb coating does reduce the accumulation of ZHS in terms of

reduced HER activity thus improves the coulombic efficiency. Even though Al_2O_3 has low HER catalytic activity, the extremely high impedance of the Al_2O_3 passivation layer prevents the reversible deposition of Zn on its surface, making Al foil unsuitable as a current collector for Zn anode.

Compared with anode current collectors, the selection of cathode current collectors in RAZIBs is more severely restricted due to more drastic pH changes and more severe corrosion at high cathode potentials. Here, we also demonstrate that Al-Nb foil is compatible when used as cathode current collectors. We assembled Zn||MnO_2 cells by using different metal substrates as cathode current collectors. Al-Nb foil, Ti mesh, and Al foil are used to support MnO_2 cathode, which are coded as Al-Nb@MnO_2, Ti@MnO_2, and Al@MnO_2, respectively. As shown in **Figure 5a**, cyclic voltammetry (CV) tests for different Zn||MnO_2 cells were scanned under a sweep rate of 0.5 mV s^{-1}. Electrochemical reactions are barely observed on the Al foil-supported MnO_2 cathode because electrons can hardly conduct through the passivated Al surface. Al-Nb foil-supported MnO_2 shows two reduction peaks at 1.20 V and 1.32 V, while Ti foil-supported MnO_2 cathode peaks at 1.23 V and 1.35 V, respectively. The difference in the peak position manifests that the electrical conductivity between the active materials and Al-Nb foil is slightly lower when compared to the Ti mesh current collector.

However, the higher peak current of the Al-Nb@MnO_2 implies that the cathodes, which use Al-Nb foil as a current collector, may have a better mass-transfer performance than the conventional Ti mesh supported MnO_2 cathode. Then we monitored the CV curves for cells that have a configuration of metal foil||Zn, and the results are shown in **Figure 5b.** The current observed in this test can represent the corrosion rate at different potentials. It is apparent that the Al foil will be strongly corroded at high potential, which can be partly ascribed to the boosted dissolution of Al metal under applied voltage and partly due to the oxygen evolution reaction (OER). The Ti mesh-related cell exhibits a rapid increase in current that starts from 1.62 V, while the current rise in the Al-Nb||Zn cell starts from 1.88 V, indicating that the Al-Nb foil has a better performance in anti-corrosion and anti-OER at high potential even when comparing it with Ti metal. Based on this result, a constant potential test was used to evaluate the damage of the three current collectors under high voltage. As shown in **Figure S17**, three different substrates were placed in Zn||metal foil cells. The Al showed a very high current and an increasing trend of dissolution during the 2V constant potential test, while the Al-Nb foil and Ti foil only shows a low and stable current. The corrosion of the three substrates after the potentiostatic test are shown in **Figure S18**, **Figure S19** and **Figure S20**. It can be seen that many holes of different sizes appear on

the surface of Al (Figure S19), while the surfaces of Al-Nb foil and Ti foil remain almost unchanged. This indicates that the corrosion rate of Al at high voltage is much faster than the other two, only Al-Nb and Ti have the potential to be used as the current collector for RAZIBs. In addition, considering the larger surface area of Ti mesh compared to other samples, the electrochemical performance of Ti foil was also tested, and it exhibited impedance characteristics and corrosion resistance properties that are very similar to those of Al-Nb (**Figure S21**). As shown in **Figure 5c** and **5d**, EIS results and the corresponding distribution of relaxation times (DRT) analysis also help prove our conclusion. Here, relaxation time τ_1, τ_2, and τ_3 are considered as contact resistance (including the solution resistance), film impedance, and charge transfer resistance, respectively. The film impedance of Ti foil is almost the same as the value of Al-Nb foil, while the charge transfer resistance of Al-Nb is slightly higher than that of Ti, which collaterally confirms the phenomenon observed in CV tests. Moreover, the influence of thickness of the Nb coating is shown in **Figure S22** and **S23**, from which we believe that the magnetron sputtering step should last for at least 5 minutes, and a longer magnetron sputtering time will bring more reliable performance. Nonetheless, the choice of the magnetron sputtering time should be adjusted according to the real-world production requirements.

In order to further investigate the possibility of using Al-Nb as cathode current collector for RAZIBs, Zn||MnO_2 cells with Al-Nb foil as cathode current collectors were tested. As shown in **Figure 6a**, the MnO_2 cathode supported by Al-Nb foil provides an initial capacity of 203.7 mAh g^{-1}, gradually increasing to 287.4 mAh g^{-1} with cycling due to the activation of electrode materials. The capacity value owned by the Al-Nb@MnO_2 cathode is close to the theoretical capacity of MnO_2, i.e., 308 mAh g^{-1} based on Mn(IV) → Mn(III), indicating that the electrochemical performance of MnO_2 cathode will not be damaged when Al-Nb is used as the current collector. As a comparison, Al@MnO_2 shows a low capacity of only 50.8 mAh g^{-1} at the first cycle. After reaching the highest capacity of around 100 mAh g^{-1}, the cathode capacity of Zn||Al@MnO_2 cell rapidly attenuates to a value lower than 10 mAh g^{-1}, indicating that not only the discharge capacity of the active material is impaired but also the cycling performance is seriously affected when Al metal is used as the cathode current collector. Voltage profiles of the Zn||Al-Nb@MnO_2 cell as shown in **Figure 6b** confirm that the overpotential shows almost no change during the 100 cycles, proving that the Al-Nb current collector does not influence the performance of the MnO_2 cathode. By comparing **Figure 6b** and **6c**, it can be found that the MnO_2 cell with Al current collector has a lower plateau voltage, which can no longer provide a normal discharge

curve at the 101st cycle. Direct observation of the as-tested current collectors can answer the problem of why the Al current collector shows a deteriorated performance after several cycles. As exhibited in **Figure 6d**, the Al current collector is severely corroded after cycling; in addition to the appearance that is no longer complete, lots of pits, which are generated by the dissolution of Al, are left on the surface. The boosted dissolution of Al may be ascribed to the dramatic changes in pH near the electrode, by which the oxide layers are repeatedly generated/dissolved due to the continuous variation between acidic and basic in interfacial pH. [40, 47] In contrast to the broken Al current collector, the Al-Nb foil can keep its intact appearance and metallic luster, and SEM observation of Al-Nb shows that it does not suffer any damage after the full-cell cycling (**Figure 6e**). The superior corrosion resistance of Al-Nb foil is attributed to the stable oxides layer on the Nb coating, which can be confirmed by the STEM observation of the tested sample (**Figure S24**), indicating that the oxides layer can help Al-Nb resist the attack from aggressive species in the water. Moreover, as the circumstantial evidence, Al-Nb foil can be immersed in a 0.1 M KOH aqueous solution for 24 h without obvious change in appearance, whereas the surface of Al foil is rapidly corroded under the same conditions (**Figure S25**).

Different types of cells are also investigated, as shown in **Figure 6f**, in which the

activated carbon (AC) based cathodes were prepared with different current collectors. The performance of the Zn||Al@AC cell is not surprisingly unstable, whereas the Zn||Al-Nb@AC cell shows a superior cyclic life span longer than 50000 cycles. In addition, the Al-Nb current collector can also successfully support vanadium dioxide (VO_2) based cathode (**Figure S26**), demonstrating that the Al-Nb foil is compatible with various active materials and is suitable for serving as cathode current collectors in RAZIBs. Moreover, Zn||Al-Nb@MnO_2 cells with different thicknesses of Nb coating were also investigated, and the results also agree with our conclusions drawn before (**Figure S27**).

Encouraged by the impressive corrosion resistance and superior electrochemical performance of Al-Nb current collector both in anode and cathode, we tried to use the Al-Nb as both anode and cathode current collectors to assemble Zn-MnO_2 full cells, intending to develop RAZIBs with good cycling stability and high energy density through using this anode/cathode dual-purpose current collector. As shown in **Figure 6g**, a Zn-MnO_2 full cell whose cathode current collector and anode current collector are both Al-Nb foil is prepared. The load of MnO_2 on the cathode is 12.4 mg cm^{-2}, which means the areal capacity of the cathode is approximately 2.5 mAh cm^{-2}. The optical photos and the SEM images of the prepared Al-Nb@MnO_2 electrode are shown in

Figure S28. Metallic Zn is pre-plated to the Al-Nb foil to prepare the Al-Nb@Zn composite anode, and the capacity of the anode is controlled 3-times to the cathode; namely, the negative/positive ratio (NP ratio, N:P) is 3:1. The Al-Nb@Zn||Al-Nb@MnO_2 cell provides an initial capacity of 199.7 mAh g^{-1}, and the capacity retention up to 120 cycles is 95.8%, which is an excellent value under this harsh measurement condition. The uniform deposition/dissolution of Zn metal protects the cell from short circuit and guarantees a high coulombic efficiency under high capacity, while the less-blocked mass transfer and charge transfer on the cathode current collector assure the highly stable cycling performance. Therefore, we believe that Al-Nb foil has the potential as a current collector for RAZIBs, and it is suitable for serving as a current collector to replace the conventional Ti mesh, Cu foil or some other materials.

To further understand the advantages of using Al-Nb as current collectors for RAZIBs, Zn||MnO_2 pouch cell was assembled by using Al-Nb foils as current collectors. The area of the pouch cell was 35 cm^2, and a high-load MnO_2 cathode (30 mg cm^{-2}, 1050 mg MnO_2 in total) was used, in which the NP ratio was also controlled to 3:1, and the SEM images of the prepared thick Al-Nb@MnO_2 electrode are shown in **Figure S29**. The open circuit voltage (OCV) of the assembled cell is 1.355 V (**Figure S30**), and the pouch cell can light up a string of small LED lights (**Figure 7a and Video S1)**. The

detailed parameters of the pouch cell can be found in **Table S1** and **Table S2.** As shown in **Figure 7b,** the pouch cell provides stable cyclic performance with an initial capacity of 258.0 mAh g^{-1} at 0.2 C (1 C = 308 mA g^{-1}). The cell shows a gradually decreased capacity during 1 C cycling, possibly due to the thick cathode that impedes the transport of ions in the cathode framework and the relatively high discharge rate (1 C, about 9.2 mA cm^{-2}) aggravates the problem. Voltage profiles that are shown in **Figure 7c** also confirm this possibility. In comparison with the healthy voltage curve of the first 20 cycles, the 80th cycle, which shows obvious pseudo capacitor characteristics, is one of the attestations that the electrode reactions only occur in the shallow layer of the electrode.[48] Nonetheless, the Zn||MnO_2 pouch cell could successfully work under such a harsh condition, notifying us that the Al-Nb foil is applicable in developing real-world RAZIBs. To show the advantages of using Al-Nb as current collectors in RAZIBs, we calculate energy densities for Zn||MnO_2 pouch cells with different current collectors based on the parameters in Table S1, Table S2, and **Table S3**, and the results are shown in **Figure 7d**. It is apparent that the use of Al-Nb brings the highest energy density to batteries even when compared with carbon paper current collector. Besides, with the increase in the mass of the active material (MnO_2), the simultaneous use of Al-Nb as the current collector for both anode and cathode can offer more than 12% gain in energy

density in comparison with the conventional Ti mesh and Cu foil current collectors (based on one-layer pouch cell). We list the details of the difference in energy densities in **Figure S30**. Considering that this technology is low-cost, easy to commercial-scale-production, and compatible with most battery optimization strategies, the use of Al-Nb is expected to facilitate the development of practical RAZIBs with high-energy-density.

3. Conclusion

In summary, by magnetron sputtering Nb coating onto Al foils, we developed a corrosion-resistant Al-Nb foil with superior electrochemical performance when employed as current collectors for RAZIBs. Nb coating acts as a barrier to prevent Al from being attacked by aggressive species in aqueous electrolytes, by which the Al-Nb foil can resist the formation of ZHS and regulate the deposition of Zn when used as an anode current collector. Additionally, it can also prevent corrosion at high potential when used as a cathode current collector. Furthermore, the cell that uses Al-Nb foil as both anode and cathode current collectors simultaneously shows superior cycling performance and improved energy density. It is worth mentioning that the preparation of Al-Nb foil is environmentally friendly and suitable for commercial-scale production. We believe this technology can be extended to various aqueous batteries in the future to promote the development of high-energy density aqueous batteries.

Experimental Section

Preparation of Al-Nb foils: First, Al foil (Hohsen, Japan) was cut to a disk whose diameter was 108 mm to fit the PVD carrier tray. The disk-shaped Al foil was then washed with surfactant and DI-water and dried in a vacuum box for 24 h. Before DC magnetron sputtering, the Al foil was sent to the chamber, which was first evacuated to less than 5×10^{-5} Pa and filled with Ar gas. During sputtering, the Ar pressure was maintained at 0.2-0.3 Pa at a constant current of 0.5 A, while the applied voltage was 250V. The deposition times were 60 s, 300 s, 900 s, and 1500 s for preparing the Al-Nb with different Nb-layer thicknesses.

Electrochemical measurements: For the Zn||metal foil cells, the metal foils, i.e., Al foils, Al-Nb foils, Cu foils, and Zn foils, were cut into disk electrodes (diameter: 10 mm). The disk electrodes were placed in a Swagelok cell, in which Al foil (or Al-Nb foil, Cu foil) was used as the working electrode, while the Zn foil was used as the counter electrode. A piece of glass fiber filter (Advantec, GA-100) was used as a separator, and 200 μL electrolyte (2 M $ZnSO_4$, i.e., 2 mol L^{-1} $ZnSO_4$ aqueous solution) of pH 4.13 was added to the cell. The cells were operated under constant current, and the cut-off voltage for Zn stripping was set to 0.5 V.

For the Zn||Al-Nb@MnO_2 cells, two-electrode Swagelok cells were prepared through putting the Zn foil, Al-Nb@MnO_2 cathode, and a piece of glass fiber separator in the cell. 200 μL electrolyte,

which consists of 2 M $ZnSO_4$ and 0.2 M $MnSO_4$ additive, was added to each cell. Constant current (CC) mode was employed for the tests, and the cut-off voltage was set at 0.8 V for discharge and 1.85 V for charge.

For the Zn||Al-Nb@AC cells, two-electrode Swagelok cells were prepared through putting the Zn foil, Al-Nb@AC cathode, and a piece of glass fiber in the cell. 200 μL electrolyte, which only contained 2 M $ZnSO_4$, was added to each cell. CC mode was employed for the tests, and the cut-off voltage was set at 0.8 V for discharging and 1.8 V for charging.

For the Zn||Al-Nb@VO_2 cells, two-electrode Swagelok cells were prepared through putting the Zn foil, Al-Nb@VO_2 cathode, and a piece of glass fiber in the cell. 200 μL 2 M $ZnSO_4$ electrolyte was used in each cell. CC mode was employed for the tests, and the cut-off voltage was set at 0.2 V for discharge and 1.4 V for charge.

For the Al-Nb@Zn||Al-Nb@MnO_2 cells, 7.5 mAh cm^{-2} Zn metal was pre-deposited onto an Al-Nb foil to prepare the Al-Nb@Zn anode. The two-electrode Swagelok cell was prepared through putting Al-Nb@Zn anode, Al-Nb@MnO_2 cathode and a piece of glass fiber in the cell. 200 μL electrolyte, which consists of 2 M $ZnSO_4$ and 0.2 M $MnSO_4$ additive, was added to the cell. CC mode was employed for the tests, and the cut-off voltage was set at 0.8 V for discharge and 1.85 V for charge.

Air-assembled Zn-MnO_2 pouch cells were constructed with the same electrodes, electrolyte, and configuration. The electrode area was set at 7 cm×5 cm. The Al-Nb@Zn anode was paired with the

Al-Nb@MnO2 cathode (active MnO_2 loading: 30.0 mg cm^{-2}). Detailed parameters are presented in Table S1, Table S2 and Table S3. Constant current-constant voltage (CC-CV) mode was employed for the tests. The cut-off voltage was set at 0.8 V for discharge and 1.8 V for charge during the CC step, while the cut-off current was set at 0.1 C for the CV step.

Other experiments, including the preparation of active materials, the preparation of cathodes, and some other electrochemical measurements, can be found in the supplemental information.

Characterization: High-resolution transmission electron microscopy (HRTEM) observation, electron energy loss spectroscopy (EELS) measurements, and elemental analysis were conducted on a Cs-corrected scanning transmission electron microscope (STEM, Titan3 G2 60-300, FEI Company). Auger electron spectra were obtained by an Auger electron spectroscopy system (JAMP-9500F). X-ray photoelectron spectra depth profiles were obtained by X-ray photoelectron spectroscopy (XPS, JEOL, JPS-9200) system, and the Mg-Kα X-ray source (hν = 1253.6 eV) was chosen. X-ray diffraction (XRD) patterns were obtained by using an X-ray diffractometer (Rigaku MiniFlex600) using Cu Ka radiation. Atomic force microscopy (AFM) tests were conducted on an AFM (Hitachi, NanonaviSII). The scanning electron microscope (SEM, ZEISS Sigma 500) was used for morphology observation, combined with the energy dispersive spectroscopy (EDS) measurements. Distribution of relaxation times (DRT) simulation was conducted by using the DRT tools. For the SEM observation of cathode current collectors, the cathodes which were used in the full-cell tests

were washed after being taken out from the cells. After drying in a vacuum oven, the portion of current collector was used for subsequent SEM observation. For the STEM observation, all the samples were prepared using an ultramicrotome (RMC Boeckeler Instruments, PowerTomeXL).

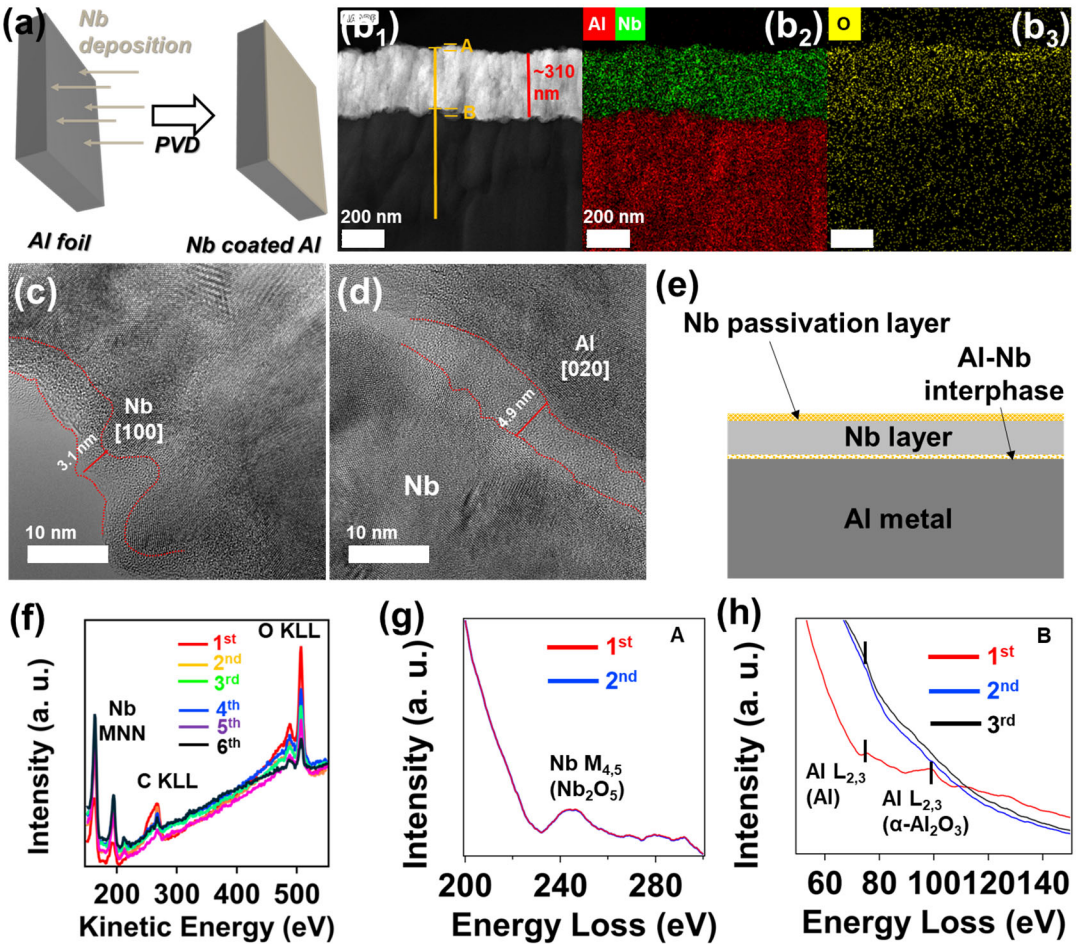

Figure 1. (a) Schematic illustration for the preparation of Al-Nb. (b_1) Cross-sectional STEM image and (b_2, b_3) the corresponding EDS mapping of the Al-Nb foil. HRTEM micrograph of (c) the Nb coating at its top surface and (d) the interface between Al substrate and Nb coating. (e) Schematic illustration for the structure of Al-Nb. (f) AES

depth profile of the Al-Nb. The EELS spectra of the Al-Nb taken from (g) the outer surface (position A, Figure 1b$_1$), and (h) the interface (position B, Figure 1b1). The orange line shown in Figure 1b1 is where to capture the EELS spectra through a linear scanning method, the distance between two sampling points is about 4 nm.

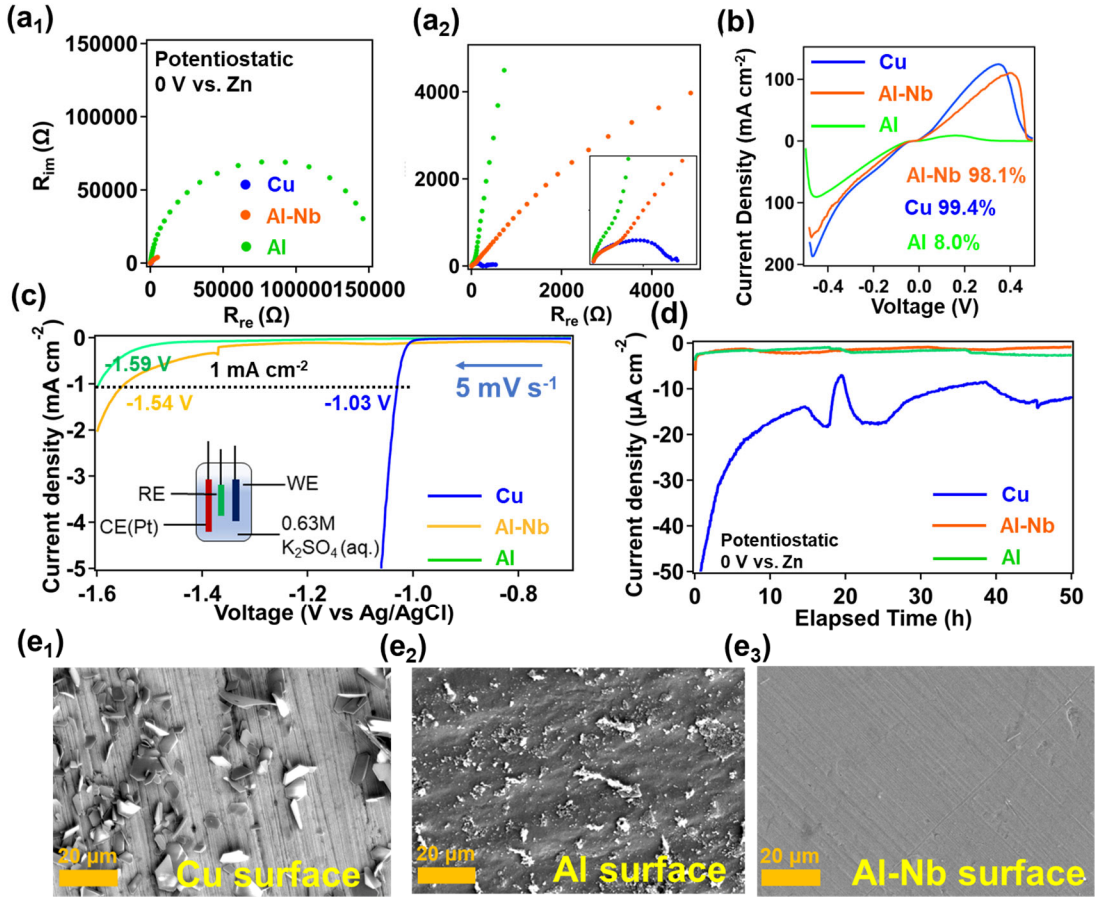

Figure 2. (a$_1$, a$_2$) Nyquist plots of different cells, Figure 2a$_2$ is the enlarged Figure 2a$_1$. (b) LSV curves of different Zn||Substrate cells. (c) LSV curves of different substrates during HER in the three-electrode cell. (d) Current-Time curves of the different metal substrates corroded under constant potential. SEM images of (e$_1$) Cu foil, (e$_2$) Al foil,

(e_3) Al-Nb foil after the potentiostatic corrosion test.

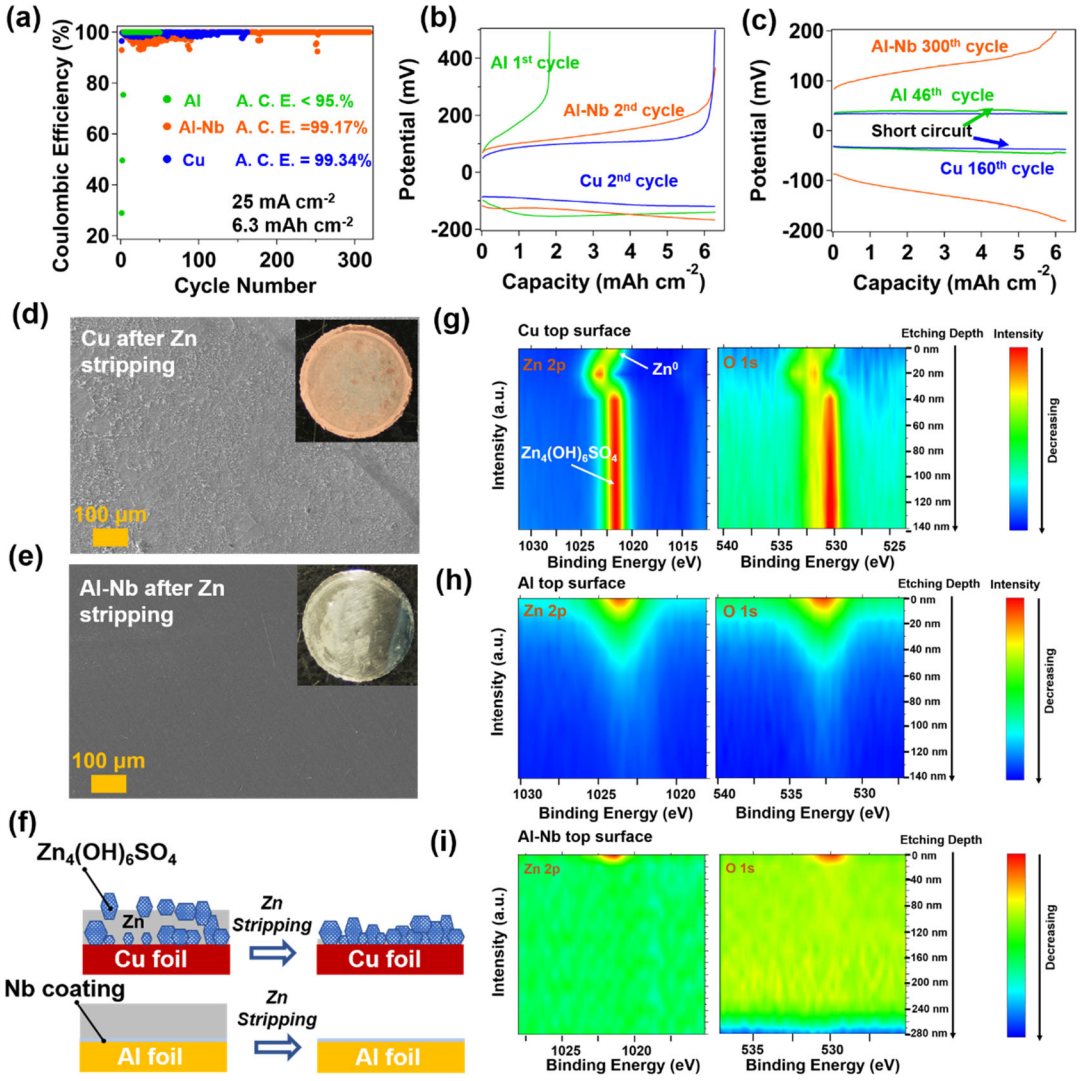

Figure 3. (a) Coulombic efficiency of Zn plating/stripping in Al||Zn (green), Al-Nb||Zn (orange) and Cu||Zn (blue) cells. Voltage profile of the half-cells at (b) early stage and (c) late stage. SEM images of (d) Cu foil after Zn stripping and (e) Al-Nb foil after Zn

stripping, the inset optical photos are the Cu foil and the Al-Nb foil after Zn stripping. (f) Schematic demonstration for the difference between Cu foil and Al-Nb foil during Zn stripping. XPS depth profile of (g) the Cu foil, (h) the Al foil and (i) the Al-Nb foil after Zn stripping.

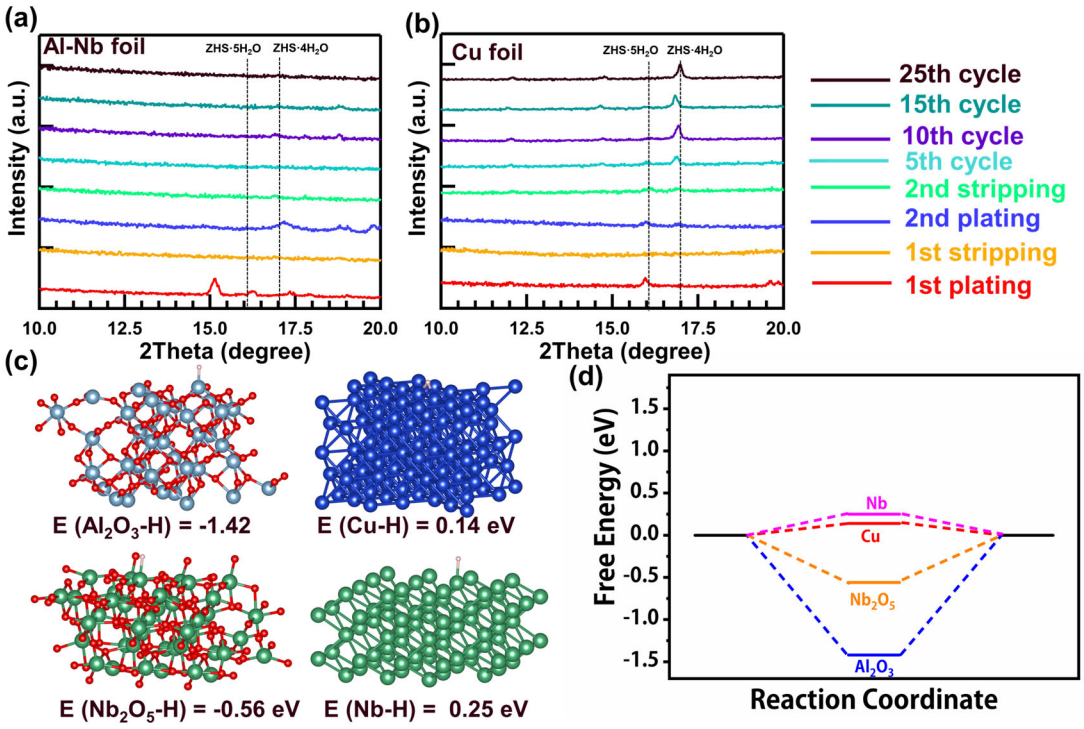

Figure 4. Ex-situ XRD patterns of different substrates after Zn plating/stripping. XRD patterns at different stage for (a) Al-Nb foil and (b) Cu foil. The plating/stripping current density is 10 mA cm^{-2} and the capacity is 5 mAh cm^{-2}. (c) The used models for DFT simulation. (d) Free-energy barriers for HER on different substrates.

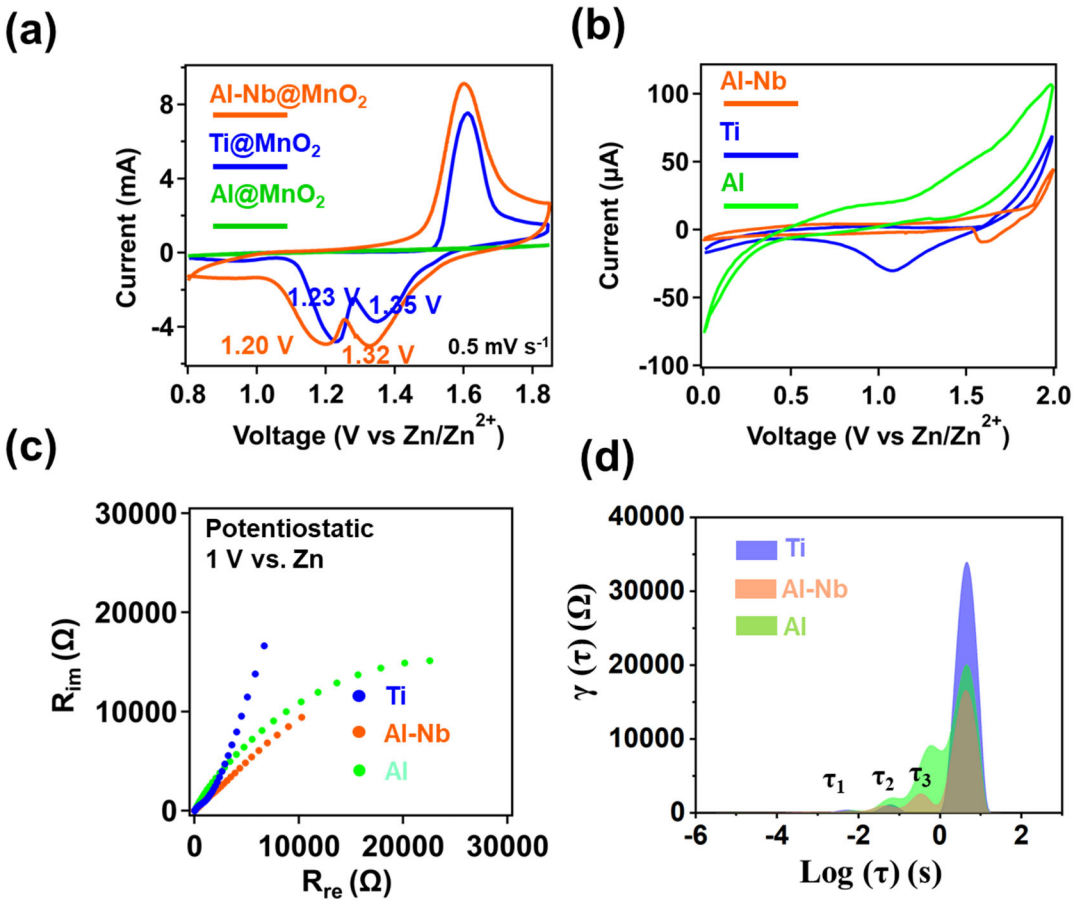

Figure 5. (a) CV curves of Zn||MnO_2 full cells at the scanning rate of 0.5 mV s^{-1}. (b) CV tests of Zn||metal foil half cells at the scanning rate of 0.5 mV s^{-1}. (c) Nyquist plots of different Zn||metal foil half cells. (d) DRT results corresponding to the Nyquist plots (Figure 5c).

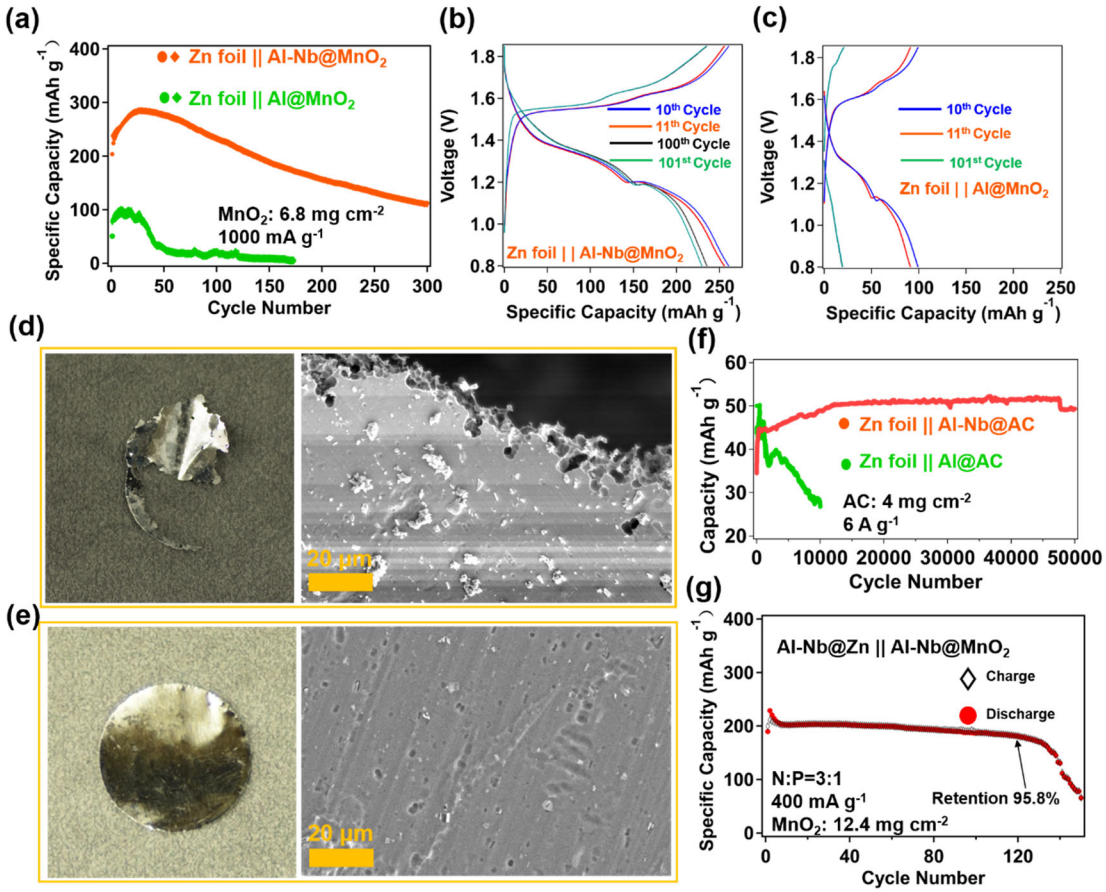

Figure 6. (a) Cycling performance of Zn||MnO_2 full cells with different cathode current collectors. Voltage profiles of Zn||MnO_2 cells with (b) the Al-Nb current collector and (c) the Al current collector. Optical photos and SEM images of (d) the Al current collector after cycling and (e)the Al-Nb current collector after cycling. (f) Cyclic performance of Zn||AC cells. (g) Cycling performance of the Zn||MnO_2 cell enabled by Al-Nb current collectors.

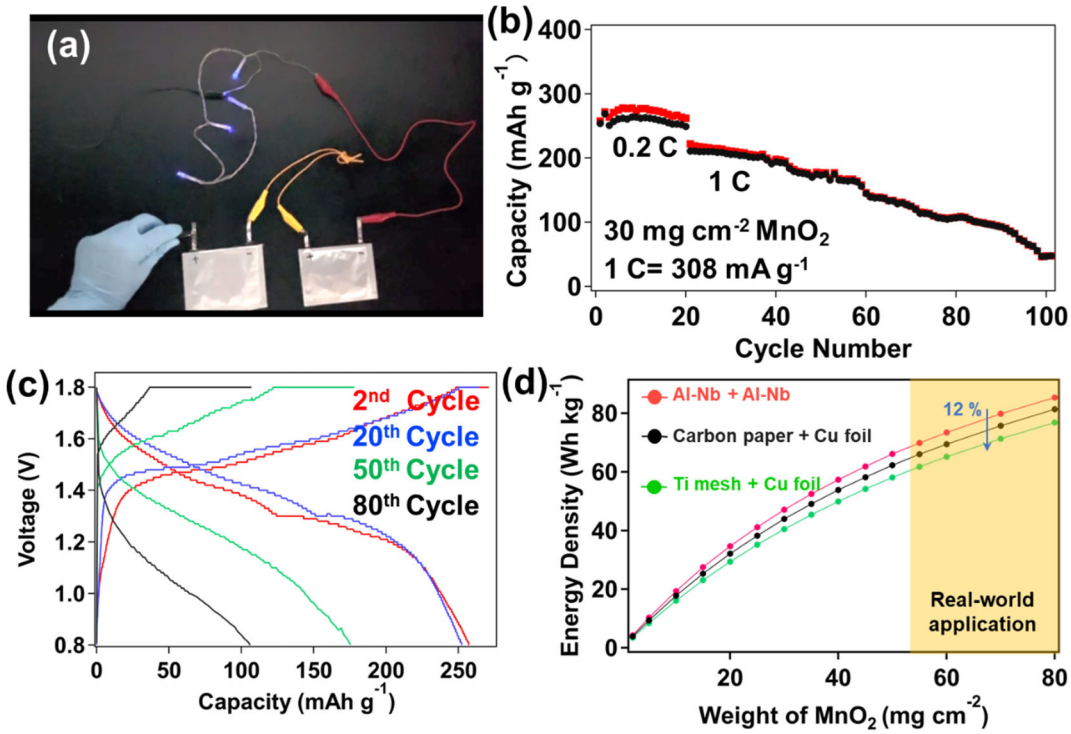

Figure 7. Electrochemical performance of Zn-MnO_2 pouch cell with Al-Nb current collectors. (a) Optical photos for illustrating lighting up a group of small LED lights. (b) Cycling performance of the Zn-MnO_2 pouch cell. (c) Voltage profiles of the pouch cell. (d) The predicted energy density of the pouch cell varies with cathode loading when different current collectors are used. The orange region indicates that the cathode loading within this area meets the demands for real-world applications.

Acknowledgements

R. Zhu and Z. Xiong contributed equally to this work.

This work was supported partially by the Japan Society for Promotion of Science (JSPS). A part of

the characterization work was conducted at Hokkaido University, supported by the “Nanotechnology Platform” Program of the Ministry of Education, Culture, Sports, Science and Technology (MEXT), Japan. R. Zhu would like to thank the support by the Program for Leading Graduate Schools (Hokkaido University “Ambitious Leader's Program”) and Grant-in-Aid for JSPS Research Fellow. C. Zhu also acknowledges the support from the National Natural Science Foundation of China (No. 52006238), the Natural Science Foundation of Jiangsu Province (No. BK20200635) and the Fundamental Research Funds for the Central University (grant no. 2020ZDPYMS24).

Conflict of Interest

The authors declare no conflict of interest.

Reference

[1] J.S. Ko, A.B. Geltmacher, B.J. Hopkins, D.R. Rolison, J.W. Long, J.F. Parker, *ACS Appl. Energy Mater.* **2018**, 2, 212-216.

[2] D. Linden, *Linden's Handbook of Batteries 4th Ed*, McGraw-Hill:New York, **2011**.

[3] N. Zhang, X. Chen, M. Yu, Z. Niu, F. Cheng, J. Chen, *Chem. Soc. Rev.* **2020**, 49, 4203-4219.

[4] P. Liang, J. Yi, X. Liu, K. Wu, Z. Wang, J. Cui, Y. Liu, Y. Wang, Y. Xia, J. Zhang, *Adv. Funct. Mater.* **2020**, 30, 1908528.

[5] H. Yang, Z. Chang, Y. Qiao, H. Deng, X. Mu, P. He, H. Zhou, *Angew. Chem. Int. Ed.* **2020**, 59, 9377-9381.

[6] P. Hu, M. Yan, T. Zhu, X. Wang, X. Wei, J. Li, L. Zhou, Z. Li, L. Chen, L. Mai, *ACS Appl. Mater. Interfaces* **2017***,* 9, 42717-42722.

[7] N. Zhang, Y. Dong, M. Jia, X. Bian, Y. Wang, M. Qiu, J. Xu, Y. Liu, L. Jiao, F. Cheng, *ACS Energy Lett.* **2018**, 3, 1366-1372.

[8] H. Yang, Y. Qiao, Z. Chang, H. Deng, X. Zhu, R. Zhu, Z. Xiong, P. He, H. Zhou, *Adv. Mater.* **2021**, 33, 2102415.

[9] Y. Zeng, X. Zhang, Y. Meng, M. Yu, J. Yi, Y. Wu, X. Lu, Y. Tong, *Adv. Mater.* **2017**, 29, 1700274.

[10] J. Fu, R. Liang, G. Liu, A. Yu, Z. Bai, L. Yang, Z. Chen, *Adv. Mater.* **2019**, 31, 1805230.

[11] J.F. Parker, E.S. Nelson, M.D. Wattendorf, C.N. Chervin, J.W. Long, D.R. Rolison,

ACS Appl. Mater. Interfaces **2014**, 6, 19471-19476.

[12] E.G. Gagnon, *J. Electrochem. Soc.* **1986**, 133, 1989-1995.

[13] J.F. Parker, C.N. Chervin, I.R. Pala, M. Machler, M.F. Burz, J.W. Long, D.R. Rolison, *Science* **2017**, 356, 415-418.

[14] S. Higashi, S.W. Lee, J.S. Lee, K. Takechi, Y. Cui, *Nat. Commun.* **2016**, 7, 11801.

[15] F. Wang, O. Borodin, T. Gao, X. Fan, W. Sun, F. Han, A. Faraone, J.A. Dura, K. Xu, C. Wang, *Nat. Mater.* **2018**, 17, 543-549.

[16] J. Xie, Z. Liang, Y.C. Lu, *Nat. Mater.* **2020**, 19, 1006-1011.

[17] A. Naveed, H. Yang, Y. Shao, J. Yang, N. Yanna, J. Liu, S. Shi, L. Zhang, A. Ye, B. He, *Adv. Mater.* **2019**, 31, 1900668.

[18] R. Zhao, Y. Yang, G. Liu, R. Zhu, J. Huang, Z. Chen, Z. Gao, X. Chen, L. Qie, *Adv. Funct. Mater.* **2020**, 31, 2001867.

[19] Y. Li, S. Wang, J.R. Salvador, J. Wu, B. Liu, W. Yang, J. Yang, W. Zhang, J. Liu, J. Yang, *Chem. Mater.* **2019**, 31, 2036-2047.

[20] Z. Guo, Y. Ma, X. Dong, J. Huang, Y. Wang, Y. Xia, *Angew. Chem. Int. Ed.* **2018**, 57, 11737-11741.

[21] X. Zeng, J. Liu, J. Mao, J. Hao, Z. Wang, S. Zhou, C.D. Ling, Z. Guo, *Adv. Energy Mater.* **2020**, 10, 1904163.

[22] D. Chao, C.R. Zhu, M. Song, P. Liang, X. Zhang, N.H. Tiep, H. Zhao, J. Wang, R. Wang, H. Zhang, H.J. Fan, *Adv. Mater.* **2018**, 30, 1803181.

[23] W. Deng, Z. Zhou, Y. Li, M. Zhang, X. Yuan, J. Hu, Z. Li, C. Li, R. Li, *ACS Nano* **2020**, 14, 15776-15785.

[24] J. Zhao, H. Ren, Q. Liang, D. Yuan, S. Xi, C. Wu, W. Manalastas, J. Ma, W. Fang, Y. Zheng, C.-F. Du, M. Srinivasan, Q. Yan, *Nano Energy* **2019**, 62, 94-102.

[25] J. Yu, F. Chen, Q. Tang, T.T. Gebremariam, J. Wang, X. Gong, X. Wang, *ACS Appl. Nano Mater.* **2019**, 2, 2679-2688.

[26] X. Wang, F. Wang, L. Wang, M. Li, Y. Wang, B. Chen, Y. Zhu, L. Fu, L. Zha, L. Zhang, Y. Wu, W. Huang, *Adv. Mater.* **2016**, 28, 4904-4911.

[27] N. Zhang, F. Cheng, Y. Liu, Q. Zhao, K. Lei, C. Chen, X. Liu, J. Chen, *J. Am. Chem. Soc.* **2016**, 138, 12894-12901.

[28] Y. Jin, L. Zou, L. Liu, M.H. Engelhard, R.L. Patel, Z. Nie, K.S. Han, Y. Shao, C. Wang, J. Zhu, H. Pan, J. Liu, *Adv. Mater.* **2019**, 31, 1900567.

[29] Q. Ni, B. Kim, C. Wu, K. Kang, *Adv. Mater.* **2022**, 34, 2108206.

[30] E.P. Banczek, P.R.P. Rodrigues, I. Costa, *Surface and Coatings Technology* **2008**, 202, 2008-2014.

[31] Y. Li, J. Xu, *Electrochimica Acta* **2017**, 233, 151-166.

[32] S. So, Y. N. Ahn, J. Ko, I. T. Kim, J. Hur, *Energy Storage Materials* **2022**, 52, 40-51.

[33] A. Mozalev, R. M. Vázquez, C. Bittencourt, D. Cossement, F. Gispert-Guirado, E. Llobet, H. Habazaki, *Journal of Materials Chemistry C* **2014**, 2, 4847-4860.

[34] J. Zähr, H.-J. Ullrich, S. Oswald, M. Türpe, U. Füssel, *Welding in the World* **2013**, 57, 449-455.

[35] N. Sato, An overview on the passivity of metals, *Corros. Sci.* **1990**, 31, 1-19.

[36] D. Bach, H. Stormer, R. Schneider, D. Gerthsen, J. Verbeeck, *Microsc. Microanal.* **2006**, 12, 416-423.

[37] Y. Cui, Q. Zhao, X. Wu, X. Chen, J. Yang, Y. Wang, R. Qin, S. Ding, Y. Song, J. Wu, K. Yang, Z. Wang, Z. Mei, Z. Song, H. Wu, Z. Jiang, G. Qian, L. Yang, F. Pan, *Angew. Chem. Int. Ed.* **2022**, 59, 16594-16601.

[38] K. Venkatraman, R. Gusley, L. Yu, Y. Dordi, R. Akolkar, Journal of The Electrochemical Society **2016**, 163, D3008-D3013.

[39] P. Xiao, H. Li, J. Fu, C. Zeng, Y. Zhao, T. Zhai, H. Li, *Energy & Environmental Science* **2022**, 15, 1638-1646.

[40] L. Godeffroy, I. Aguilar, J. Médard, D. Larcher, J.M. Tarascon, F. Kanoufi, *Adv. Energy Mater.* **2022**, 2200722.

[41] J. Zheng, Z. Cao, F. Ming, H. Liang, Z. Qi, W. Liu, C. Xia, C. Chen, L. Cavallo, Z. Wang, H.N. Alshareef, *ACS Energy Lett.* **2021**, 7, 197-203.

[42] R. H. Yoon, T. Salman, G. Donnay, *J. Colloid Interface Sci.* **1979**, 70, 483.

[43] D. A. Sverjensky, *Geochim. Cosmochim. Acta* **1994**, 58, 3123.

[44] M. Kosmulski, *Langmuir* **1997**, 13, 6315-6320.

[45] R. Zhu, Z. Xiong, H. Yang, T. Huang, S. Jeong, D. Kowalski, S. Kitano, Y. Aoki, H. Habazaki, C. Zhu, *Energy Storage Materials* **2022**, 46, 223-232.

[46] H. Liu, Y. Zhang, C. Wang, J.N. Glazer, Z. Shan, N. Liu, *ACS Appl. Mater. Interfaces* **2021**, 13, 32930-32936.

[47] S. Gheytani, Y. Liang, Y. Jing, J.Q. Xu, Y. Yao, *J. Mater. Chem. A* **2016**, 4, 395-399.

[48] R. Zhu, H. Yang, W. Cui, L. Fadillah, T. Huang, Z. Xiong, C. Tang, D. Kowalski, S. Kitano, C. Zhu, D.R. King, T. Kurokawa, Y. Aoki, H. Habazaki, *J. Mater. Chem. A* **2022**, 10, 3122-3133.